KSCE Journal of Civil Engineering (2019) 23(8):3571-3580

DOI 10.1007/s12205-019-1921-1

**Structural Engineering**

pISSN 1226-7988, eISSN 1976-3808
www.springer.com/12205

# Analysis of Mechanical Characteristics of Steel-Concrete Composite Flat Link Slab on Simply-Supported Beam Bridge

**Chengquan Wang***, **Yonggang Shen****, **Yun Zou*****, **Yizhou Zhuang******, **and Tianqi Li*******

Received October 25, 2018/Revised March 21, 2019/Accepted May 1, 2019/Published Online July 8, 2019

## Abstract

Based on linear elastic theory, the concrete cracking problem of link slab on simply supported beam bridge was explored and theoretical analysis of bridge link slabs were carried out. Meanwhile, the formulas for calculating the stress of link slab were deduced and the cause for continuous damage of bridge deck was quantitatively analyzed. On the base of analysis of its failure mechanism, a new type of steel-concrete composite flat link slab was proposed. The results of full-scale model tests and finite element (FE) analysis indicated that it can alter the transfer path of internal forced inside the link slab and then concrete cracking can be prevented effectively. It was found that the main factors to link slab failure were influentially descending from girder end upturning, longitudinal tensile action and girder end rotation. Furthermore, the unbonded region between girder and link slab can effectively decrease the continuous stress and then alleviate the damage to bridge deck. All those results in this paper can be used as a reference and guidance for further research and development of new type of bridge link slab and jointless bridge.

Keywords: *mechanical characteristic, model test, simply supported beam bridge, steel-concrete composite flat link slab, theoretical derivation*

## 1. Introduction

The simply supported beam bridges with link slab have the advantages of simple structure, definite stress and convenient construction, and the link slab can lead to the jointless bridge deck in the simply supported beam bridge, which can avoid the bridge diseases and high maintenance costs caused by the bridge expansion joints. Therefore, the link slab has been widely used in small and medium span bridges. The concept of the link slab of simply-supported beam bridges was first proposed in the late 1970s (Loveall, 1985), which connecting the bridge deck as a whole instead of setting up special telescopic devices between two girders. This simply-supported beam bridge with link slab not only has the mechanical characteristics of simply-supported beam bridge, but also has good driving stability and driving comfort. However, in the process of bridge operation, there are many cracks in the bridge slab-deck, which not only affected the ride comfort, but also caused a series of diseases, such as bridge corrosion (Badie *et al.,* 2001; Oesterle *et al.,* 2004; Okeil and Elsafty, 2005; Attanayake *et al.,* 2008; El-Safty, 2008). In 1998, Alampalli and Yannotti (1998) investigated the deck of 105 bridges (including the concrete girder bridge and the 33 steel girder bridges) in the United States of America, and found that almost all of the bridge decks continuously cracked, these diseases significantly increased the cost of bridge maintenance.

In order to reduce the continuous deck damage, many scholars have explored the damage reasons and proposed improvements. Okeil and Elsafty (2005) compared the data from the experimental and FE analysis with the existing data in the literature, and explored the effect of the bridge deck pavement material stiffness on the angle of the continuous slab-deck (link slab), the angle formula of the continuous slab-deck (link slab) section under the static load was also derived. Kendall *et al.* (2008) and Lepech and Li (2009) researched on the continuous slab-deck (link slab) made of engineered cementitious composites (ECC) concrete, and found that the material properties of ECC is better than the general continuous slab-deck (link slab) concrete, the use of ECC material can improve bridge deck constructability, durability, and sustainability. Gastal and Zia (1989) designed the FE program and established the related bridge FE model, analyzed the effect of the static load on the mid-span bending moment and the deflection of the simply-supported beam bridge with link slab. Strauss *et al.* (2012), Moradi *et al.* (2016), Moradi *et al.* (2017), Zheng *et al.* (2018) added the fiber reinforced

*Research Assistant Professor, School of Environment and Civil Engineering, Jiangnan Univeristy, Wuxi 214122, China (Corresponding Author, E-mail: drwcq@jiangnan.edu.cn)
**Associate Professor, Dept. of Civil Engineering, Zhejiang Univeristy, Hangzhou 310058, China (E-mail: sygdesign@163.com)
***Professor, School of Environment and Civil Engineering, Jiangnan Univeristy, Wuxi 214122, China (E-mail: zouyun_22@126.com)
****Professor, School of Civil Engineering and Architecture, Zhejiang University of Technology, Hangzhou 310014, China (E-mail: 478372092@qq.com)
*****Associate Professor, School of Environment and Civil Engineering, Jiangnan Univeristy, Wuxi 214122, China (E-mail: ltq_tiger15@126.com)

plastic (FRP) into the link slab, the results of a large number of simulations and tests showed that using the FRP material in link slab can not only decrease the moment and angle of the beam end, the damage extent of link slab are also obviously reduced. Sevgili and Caner (2009) simulated the different connection modes of connecting bar in link slab with FE method from observation and analysis of the simply-supported beam bridges with link slab in Turkey highway, on this basis, modeled the two-span 18m and four-span 25m continuous deck simply-supported beam bridge, then obtained the changes of girder angle under static loads with different bar connection modes and different spans. Wang *et al.* (2000) analyzed the deformation and stress of the link slab on simply-supported beam bridge under live load and temperature and derived the corresponding formulas. Li *et al.* (2012) analyzed linear elastic theory the continouse paving layer under the live load, temperature variation, and the deformation and tensile stress formulations of link slab were derived. Chang He and Zhong-fu Xiang (2005) increased the diameter of the continuous deck rebar and adopted the modified epoxy concrete with low elastic modulus in the link slab to improve the crack resistance, and modeled the FE model to analyze the improvement of continuous deck structure stress performance. Wang *et al.* (2014), Wang *et al.* (2016) proposed a continuous structure of arch link slab, and proved that this new link slab can effectively reduce the tensile stress of concrete by model test and bridge test.

The above studies showed that the current failure mechanism cannot explain the deck concrete cracking and still needs systematic research. In this paper, both theoretical and FE analysis on the mechanical characteristics of link slab on simply supported beam bridge were made and the main factors contributing for bridge link slab failure were explored.

## 2. Failure Mechanism of Link Slab

At present, a rather large number of small and medium span bridges are simply supported beam bridges with link slabs on deck, where the debonded rebar link slab (DRLS) is most widely used in China (Wang *et al.,* 2000; Li *et al.,* 2012; Zhan *et al.,* 2013) as shown in Fig. 1. In Europe, Canada and United States, the link slab structure is mainly composed of debonded link slab (DLS) (Au *et al.,* 2013; Ghatefar *et al.,* 2015; Hossain *et al.,* 2015; Natário *et al.,* 2015; Valipour *et al.,* 2015) as shown in Fig. 2.

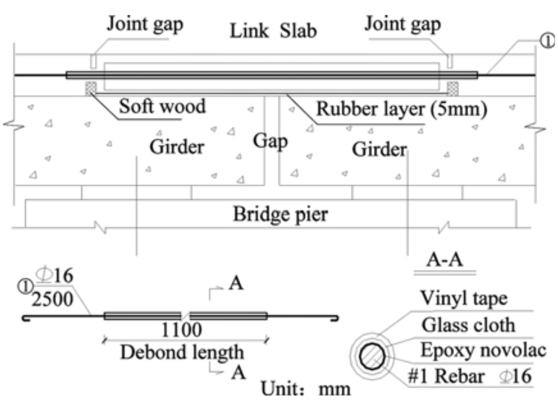


Fig. 1. Structure Diagram of DRLS

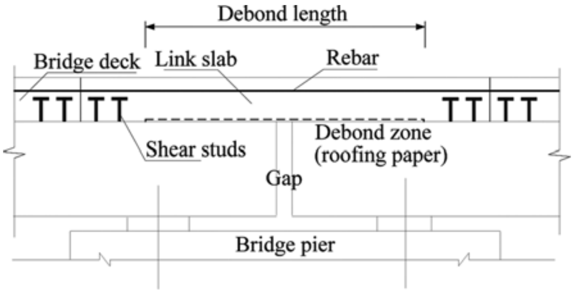


Fig. 2. Structure Diagram of DLS

The link slab on a bridge is located above the beam gap of the simply supported beam bridge, and its location and relatively weak structure results in its stress characteristics and the particularity of the failure factors. Through the analysis and summary, the

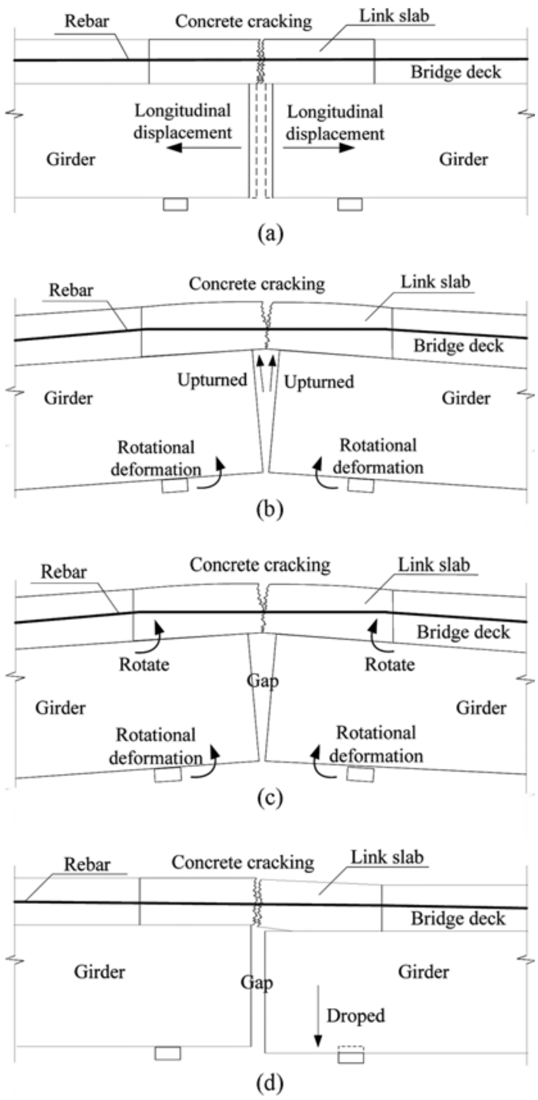


Fig. 3. Failure Factors of Bridge Link Slab: (a) Longitudinal Displacement of Beams, (b) Upturning of Beam Ends, (c) Rotation of Girders, (d) Differential Settlement

deformation of the link slab under the external load was mainly the following four kinds, as shown in Fig. 3.

The main deformation caused by the concrete cracking of bridge link slab was the axial tensile force caused by temperature or live load of girder (Fig. 3(a)), the upturned and rotational extrusion deformation of the girder end induced by live load and temperature gradient (Figs. 3(b) and 3(c)), and the vertical shear action led by the vertical dislocation on both sides of bridge link slab (Fig. 3(d)). In the actual bridge, the link slab is often subject to a variety of loads and displacements, only by strengthening improvement or repair measures cannot avoid or solve these destructive factors fundamentally. The link slab is a part of bridge deck structure, which has been affected by deformation of the girder end in the normal use process, the destructive factors should be quantitatively analyzed to find out the main damage factors, and then put forward targeted crack prevention measures.

## 3. Theoretical Analysis of Stress Characteristics of the Bridge Link Slab

### 3.1 Theoretical Analysis of Link Slab under Bridge Load

Under the action of midspan load or bridge temperature gradient, the deformation of the link slab caused by the rotation deformation of girder end was shown in Fig. 4.

It can be seen from Fig. 4 that the deformation of link slab includes the longitudinal deformation and the rotational deformation at the connection of bridge girder, the corresponding force calculation model of the link slab was shown in Fig. 5, where, $\theta$ is the deflection angle of the main girder, $a$ is the distance from the bearing to the girder end, $H$ is the height of the girder, $\alpha$ is the angle of the bottom edge of the link slab above the bridge gap, $h$ is the thickness of the link slabs.

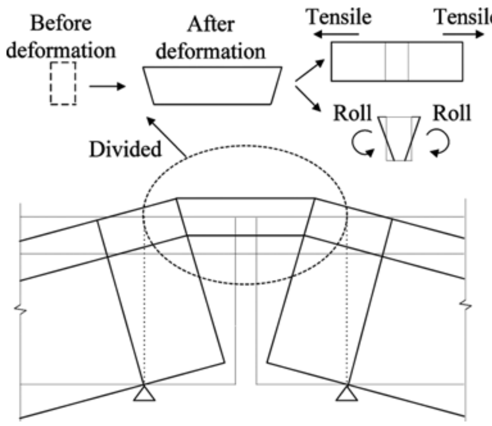


Fig. 4. Link Slab Deformation Caused by the Rotational Deformation

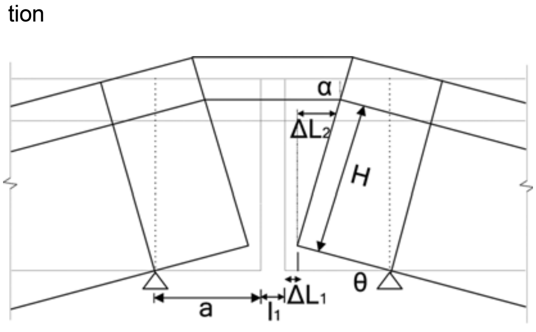


Fig. 5. Force Calculation Model of Link Slab under the Rotation Deformation

Because the link slab was poured with the main girder surface, so it can be seen from the Fig. 5 that the rotational deformation of link slab equal to the deflection angle of the main girder, i.e., $\theta = \alpha$, thus the longitudinal tensile deformation of the lower edge of the girder end is calculated as follows:

$$\Delta L_1 = a(1-\cos\theta) \tag{1}$$

The longitudinal tensile deformation of the upper edge of the girder end is obtained:

$$\Delta L_2 = (H + h/2)\sin\alpha \tag{2}$$

The calculation formula of longitudinal tensile deformation at one side of the link slab is as follows:

$$\Delta L = \Delta L_1 + \Delta L_2 = a(1-\cos\theta) + (H + h/2)\sin\theta \tag{3}$$

Under the bridge loads, the longitudinal tensile deformation of the link slab is the sum of the longitudinal deformation on both sides. Assuming that the rotation angles of the main girders on both sides are the same, the stress induced by the longitudinal tensile force can be deduced:

$$\sigma_1 = E_c\varepsilon = \frac{E_c 2\Delta L}{l_1} = \frac{2E_c\left[a(1-\cos\theta) + (H+h/2)\sin\theta\right]}{l_1} \tag{4}$$

The stress caused by the rotation deformation of the connection region between the link slab and the main girder is obtained.

$$\sigma_2 = \frac{M}{W_z} = \frac{M}{bh^2/6} \tag{5}$$

Where, $M = \frac{4E_cI_c\alpha_R}{l_1} + \frac{2E_cI_c\alpha_L}{l_1}$, $\alpha_R$, $\alpha_L$ is the right and left rotation angles of the link slab, respectively. $I_c$ is the rotational inertia of the link slab with width of $b$.

Therefore, under the deformation condition shown in Fig. 5, the tensile stress on the upper surface of the link slab is calculated as follows.

$$\sigma_{up} = \sigma_1 + \sigma_2 \tag{6}$$

The stress on the lower surface of the link slab is calculated as follows,

$$\sigma_{down} = \sigma_1 - \sigma_2 \tag{7}$$

From the above analysis, it can be concluded that the upper surface of the link slab will produce tensile stress under the rotation of the main girder. Constructing the unbonded region between the link slab and girder can not only reduce the rotation effect on the link slab and keep $\alpha < \theta$, but also increase $l_1$, thus effectively reduce the tensile stress of the upper surface.

Taking the whole structure of link slab as the research object and not limited to the upper part of the bridge gap, as shown in Fig. 6, it

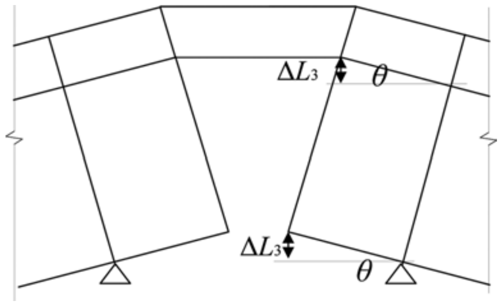


Fig. 6. Force Calculation Model of Link Slab under the Upturning Deformation

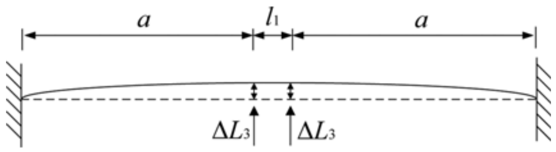


Fig. 7. Calculation Sketch Map of the Link Slab under the Upturning Deformation

can be seen that the upward bending of girder end will cause deformation ($\Delta L_3$) and stress on the link slab above the main girder.

It can be obtained from the geometric deformation relation in Fig. 6, $\Delta L_3 = a{\cdot}\sin\theta$, the force model of the link slab under the action of upturned deformation can be simplified as a beam structure in which a certain displacement occurs in midspan and is fixed at both ends, the calculation sketch map was shown in Fig. 7.

The bending moment of the central part of the link slab under $\Delta L_3$ can be obtained by mechanical deduction:

$$M_3 = \frac{24E_cI_c\Delta L_3}{a^2} \tag{8}$$

Therefore, the stress on the upper surface of the link slab is:

$$\sigma_3 = \frac{M_3}{W_z} = \frac{12E_c\sin\theta}{a} \tag{9}$$

According to the calculation of simply supported beam under midspan load, the girder end angle can be obtained:

$$\theta = \frac{PL^2}{16E'I'} \tag{10}$$

where, $P$ is equivalent midspan load of single span, $E'$ is the elastic modulus of the girder, $I'$ is the inertial moment of the girder section, and $L$ is the calculation span.

According to the Eqs. (4), (5) and (9), three stresses can be obtained, the quantitative analysis was carried out. First, the following three participation coefficients were defined:

Participation coefficient of longitudinal deformation:

$$\alpha_1 = \frac{\sigma_1}{\sigma_1+\sigma_2+\sigma_3} = \frac{\dfrac{2E_c\left[a(1-\cos\theta)+H\cdot\sin\theta\right]}{l_1}}{\dfrac{2E_c\left[a(1-\cos\theta)+H\cdot\sin\theta\right]}{l_1}+\dfrac{3E_c\alpha h}{l_1}+\dfrac{12E_c\sin\theta}{a}} \tag{11}$$

Participation coefficient of rotational deformation:

$$\alpha_2 = \frac{\sigma_1}{\sigma_1+\sigma_2+\sigma_3} = \frac{\dfrac{3E_c\theta h}{l_1}}{\dfrac{2E_c\left[a(1-\cos\theta)+H\cdot\sin\theta\right]}{l_1}+\dfrac{3E_c\alpha h}{l_1}+\dfrac{12E_c\sin\theta}{a}} \tag{12}$$

Participation coefficient of upturned deformation:

$$\alpha_3 = \frac{\sigma_1}{\sigma_1+\sigma_2+\sigma_3} = \frac{\dfrac{12E_c\sin\theta}{a}}{\dfrac{2E_c\left[a(1-\cos\theta)+H\cdot\sin\theta\right]}{l_1}+\dfrac{3E_c\theta h}{l_1}+\dfrac{12E_c\sin\theta}{a}} \tag{13}$$

In order to quantify the three failure factors, the design parameters of 20 m hollow slab bridge are taken as an example, according to the design load of highway grade I in Chinese code for design of highway reinforced concrete and prestressed concrete bridges and culverts, the equivalent mid span concentrated force $P$ is equal to 207.5 kN, the elastic modulus of girder concrete $E' = 3.45 \times 10^4$ MPa, the inertial moment of the girder section $I' =$ m$^4$, the calculation span $L = 19.3$ m, the design parameters of link slab include $E_c = 3.25 \times 10^4$ MPa, $a = 0.35$ m, $L_1 = 0.74$ m. After substituting the above design parameters in Eq. (10), it can be obtained by $\theta = 0.159^{\circ}$, then according to Eqs. (11) – (13), the participation coefficients are respectively: $\alpha_1 = 27.05\%$, $\alpha_2 = 12.47\%$, $\alpha_3 = 60.48\%$. It can be concluded that the leading destructive factor is girder end upturn, the second is the longitudinal tensile action, and the last is the girder end rotation.

## 3.2 Theoretical Analysis of Link Slab under Unbalanced Loading on Bridge

The part of the link slab above the bridge gap was taken as analysis object, when the bridge is partial load or the deformation on both sides of the girder end are inconsistent, the bending effect of girder end will further increase the tensile stress on the upper surface of the link slab, as shown in Fig. 8.

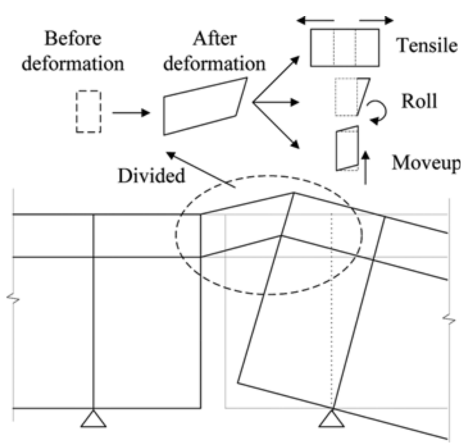


Fig. 8. Link Slab Deformation Caused by Upturned of Girder End

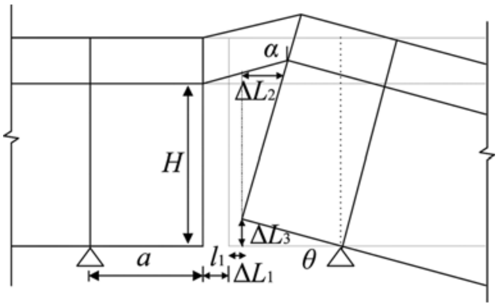


Fig. 9. Force Calculation Model of Link Slab under Upturned of Girder End

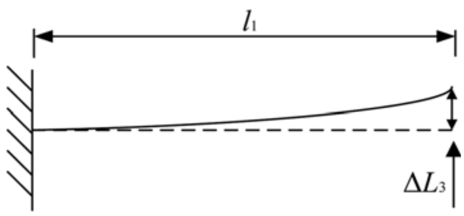


Fig. 10. Calculation Sketch Map of Link Slab under the Upturned Deformation

In the Fig. 8, under upturned of girder end, the deformation of the link slab composed of longitudinal tensile deformation, rotational deformation and upward deformation. It is assumed that the angle of a single girder end is $\theta$, the force calculation model was shown in Fig. 9, The rotational deformation of link slab equal to the deflection angle of the main girder $\alpha = \theta$, the calculated value of the upward deformation of the link slab is obtained from the geometric relationship in the Fig. 10.

The stress induced by the upturned deformation can be deduced:

$$\sigma_3 = \frac{M}{W_z} = \frac{M}{bh^2/6} \tag{14}$$

where, $M = \dfrac{6EI\Delta L_3}{l_1^2}$ .

Then the following three participation coefficients can be defined,

Participation coefficient of longitudinal deformation:

$$\alpha_1 = \frac{\sigma_1}{\sigma_1+\sigma_2+\sigma_3} = \frac{\dfrac{E_c[a(1-\cos\theta)+H\cdot\sin\theta]}{l_1}}{\dfrac{E_c[a(1-\cos\alpha)+H\cdot\sin\theta]}{l_1}+\dfrac{3E_c\alpha h}{2l_1}+\dfrac{3E_c\sin\theta}{l_1}} \tag{15}$$

Participation coefficient of rotational deformation:

$$\alpha_2 = \frac{\sigma_2}{\sigma_1+\sigma_2+\sigma_3} = \frac{\dfrac{3E_c\theta h}{2l_1}}{\dfrac{E_c[a(1-\cos\theta)+H\cdot\sin\theta]}{l_1}+\dfrac{3E_c\theta h}{2l_1}+\dfrac{3E_c\sin\theta}{l_1}} \tag{16}$$

Participation coefficient of upturned deformation:

$$\alpha_3 = \frac{\sigma_3}{\sigma_1+\sigma_2+\sigma_3} = \frac{\dfrac{3E_c\sin\theta}{l_1}}{\dfrac{E_c[a(1-\cos\theta)+H\cdot\sin\theta]}{l_1}+\dfrac{3E_c\theta h}{2l_1}+\dfrac{3E_c\sin\theta}{l_1}} \tag{17}$$

After substituting the above design parameters in Eq. (10), it can be obtained by $\theta = 0.159^{\circ}$, then according to Eqs. (15) – (17), the participation coefficients are respectively: $\alpha_1$ = 18.99%, $\alpha_2$ = 8.76%, $\alpha_3$ = 72.25%.

From the above analysis, the effect of upturned will greatly increase the tensile stress on upper surface of the link slab, if there is a certain space in lower surface of the link slab, which can avoid the upturned deformation directly and greatly reduce the tension stress on upper surface.

## 4. Introduction and FE Analysis of Steel-concrete Composite Flat Link Slab

Based on the analyses above, a new type of steel-concrete composite flat link slab (SCC-FLS) was proposed, as shown in Fig. 11. Its inside region contacted to girder end is hollow, which provides space for girder's upturned displacement and avoids the negative moment causing by the upper deck pushing. The steel plate can slip longitudinally on the smooth PTFE plate at its bottom, thus releasing the stress of concrete caused by horizontal, vertical and rotational displacements. The split gap makes the concrete of bridge deck and connecting slab completely disconnected, and the tension produced by girder deformation is transmitted by longitudinal welded steel rebars instead of concrete,

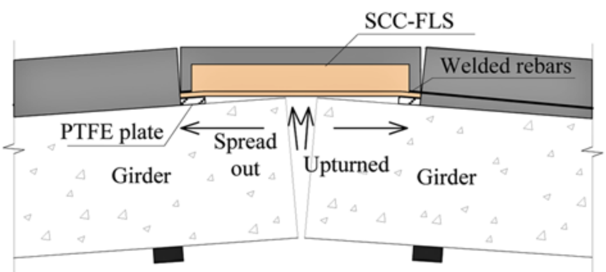


Fig. 11. Force Transmission and Deformation Principles of SCC-FLS

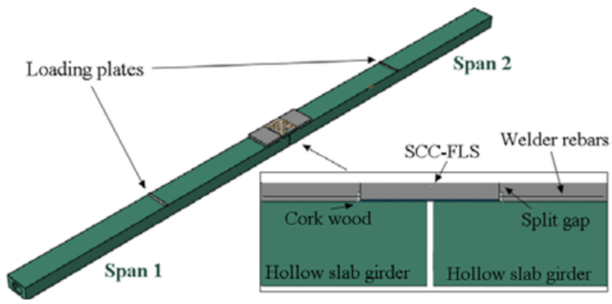


Fig. 12 FE Model of the SCC-FLS

thus avoiding the tension cracking of the upper concrete of link slab.

### 4.1 SCC-FLS FE Model Description

In order to verify the mechanical properties and whether SCC-FLS can avoid the three destructive factors mentioned above. The general-purpose finite element program ABAQUS was used in this paper to build the SCC-FLS FE model, the composition of the FE model was shown in Fig. 12, the link slab was arranged between the two spans, and the hollow slab gider was used for each span.

The 8-node brick elements with three translation degrees of freedom attach node (C3D8R) were used to model the steel plate, PTFE plate and concrete; Truss element (T3D2) is the linear component can only withstand tensile and compressive loads in space, which was used to simulate the stirrups and steel rebars (Wang *et al.,* 2016). The mesh of concrete and steel were refined, adequate size and number of elements were selected by performing mesh convergence study on some FE models. The minimum mesh size was 0.03, there were 21206 solid elements and 2080 truss elements in FE model, and the sweep meshing technique was adopted.

The damage-plasticity model was used in the FE model for simulate the concrete, the value of dilation angle ($\psi$) was 35°, which was determined by Eq. (18), the flow potential eccentricity was taken as the default value of 0.1. Calculated by Eq. (19) the ratio of the compressive strength under biaxial loading to uniaxial compressive strength ($f_{b0}/f_{c0}$) was 1.16, Invariable stress ratio ($K_c$) was calculated by Eq. (20), which was 0.667, the visosity parameter was 0.0005 (Pons *et al.,* 2018).

$$\psi = \begin{cases} 56.3(1-\xi) & \text{for } \xi \le 0.5 \\ 6.672e^{\frac{7.4}{4.64+\xi}} & \text{for } \xi > 0.5 \end{cases} \tag{18}$$

$$K_c = \frac{5.5}{5+2(f_c')^{0.075}} \tag{19}$$

$$f_{bo}/f_c' = 1.5(f_c')^{-0.075} \tag{20}$$

The relation model Saenz was used to simulate the concrete uni-axial compression stress and strain relations, which is shown in Fig. 13. The constitutive relationship of steel plate, steel rebar

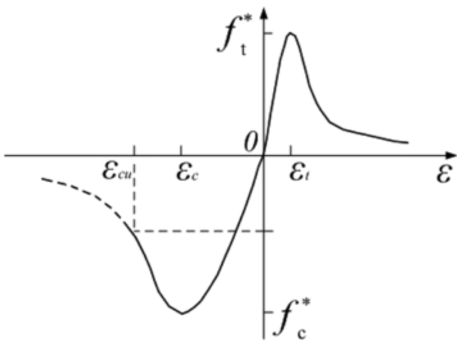


Fig. 13. FE Model of the SCC-FLS

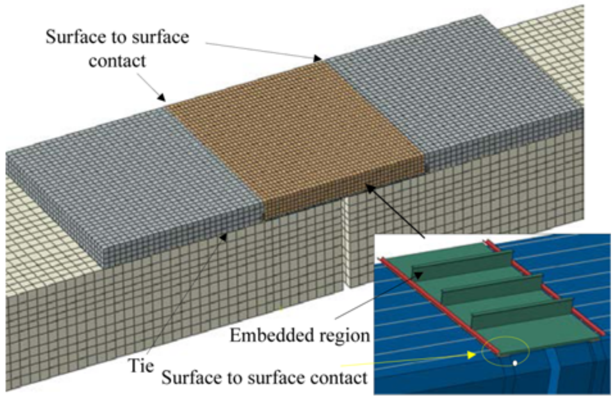


Fig. 14. FE Model of the SCC-FLS

is perfectly plastic model.

Embedded region method was attached to simulate the relationship between T-rib in SCC-FLS, steel mesh reinforcement and concrete, which was shown in Fig. 14. Surface-to-surface contact was used for the interaction simulation of the split gap, which includes normal contact and tangential slip, and a surface-based interaction with hard contact in the normal direction, the small sliding and the coulomb friction coefficient of 0.4 in the tangential direction to the interface is used to simulate the interfacial behavior, in which the sliding formulation is finite sliding. Tie constraint can couple two separate surfaces so that no relative motion occurs between them. As Fig. 14 shown, the tie option was adopted for the constraint between concrete, steel section, PTFE plate and the loading plates. The translational degrees of freedom of all nodes in the loaded steel plate are coupled in the vertical loading direction, and load was applied by means of displacement. Both material and structural nonlinearities were considered, the Static General Method was used in the solution process.

### 4.2 Analysis of SCC-FLS under Vehicle Load

In order to analyze the stress distribution on the SCC-FLS under the vehicle load, the rear axle of the loaded vehicle was placed at the mid-span of the bridge, the load application area was 60 cm × 20 cm, the appropriate location of the central axle and front axle was determined by the specifications.

It can be seen from Table 1, under the vehicle load, the stress of the concrete at the surface of the SCC-FLS was small and was compressive stress, which can be explained that the steel plate provided space to avoid the girder end pushing the upper deck; in addition, the girder longitudinal displacement made joint shrink,

Table 1. Longitudinal Stress of Concrete Top Surface under the Vehicle Load/MPa

| Type of link slab | Longitudinal stress |
|---|---|
| DRLS | 2.35 |
| DLS | 1.54 |
| SCC-FLS | -0.23 |

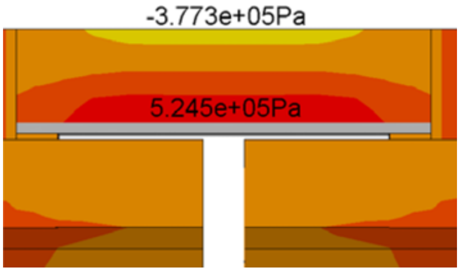


Fig. 15. Longitudinal Stress in SCC-FLS under Vehicle Load

and the joint with the steel-plate inside could make the joint pass the passive stress and finally the SCC-FLS was in compression. The stress cloud figure in Fig. 15 intuitively showed that the concrete stress of SCC-FLS was smaller and the concrete didn't crack, moreover, due to the steel plate can slide on PTFE bearing and the welding longitudinal rebars can bear tensile force, the lower edge concrete become in tension and upper edge concrete in compression. Therefore, the steel plate-type have better crack control performance.

### 4.3 Analysis of SCC-FLS under Bridge Thermal Gradient

In order to analyze the stress change in SCC-FLS under temperature effect, the temperature coefficient of concrete and steel were set in the FE model, and then the temperature field calculation of the bridge model was applied. Comparison of the FEM results of the steel-concrete composite flat link slab and two link slabs were listed in Table 2.

As can be seen from Fig. 16, when the bridge became overall warming, the mid-span of two girders down-warded and the end upturned, the upper concrete was in compression, while the new steel-concrete composite flat link slab provided enough space, so the girder end upturned would not push the link slab which avoided the negative moment generated in link slab, so the concrete stress in SCC-FLS was smaller under the vehicle load

Table 2. Longitudinal Stress of Concrete Top Surface under Temperature Gradient/MPa

| Loading conditions | Overall warming 30℃ | Overall cooling 30℃ |
|---|---|---|
| DRLS | -8.08 | 2.55 |
| DLS | -5.08 | 6.67 |
| SCC-FLS | -2.51 | 0.72 |

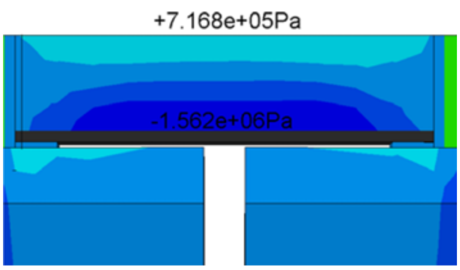


Fig. 16. Longitudinal Stress of SCC-FLS under Bridge Temperature Gradient

condition and overall warming condition, while the concrete tensile stress in DRLS and DLS were beyond the tensile strength of the concrete.

## 5. Field Test of SCC-FLS

### 5.1 Introduction of the Full-Scale Model Test

In order to verify the effect of the SCC-FLS in the actual bridge, a full-scale SCC-FLS was installed in the gap between the 2 hollow slab girders, as shown in Fig. 17 and Fig. 18. The height and width of the prestressed concrete hollow slab girder was 55 cm and 1 m, respectively, and the span was 12.6 m. The distance between the center line of the bearing and the girder end was 33 cm, and the concrete grade of the girder was C50, the concrete grade of the SCC-FLS and bridge deck was C40.

There were four concrete strain gauges set on the concrete surface of the link slab along the width direction, the steel bar strain gauges were used to measure the longitudinal stress of the welded rebar in the loading test, the layout of strain measuring

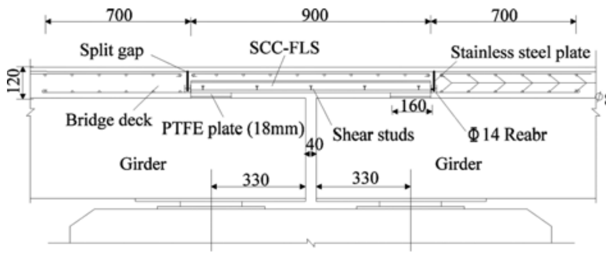


Fig. 17. Structure Diagram of the SCC-FLS/mm

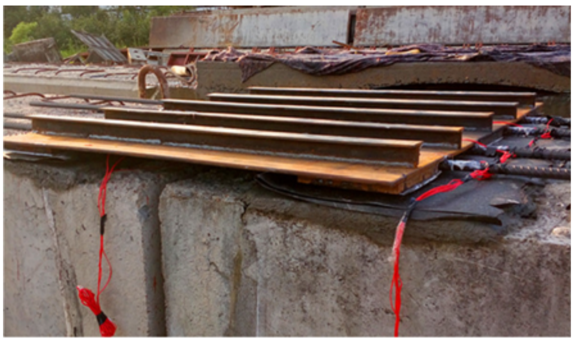

Fig. 18. Photos in Specimen Preparation

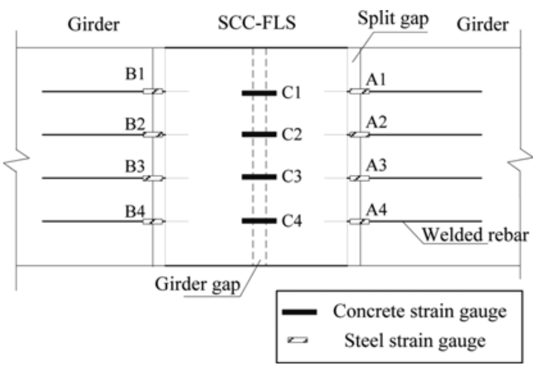


Fig. 19. Layout of Strain Measuring Points

Fig. 20. Photo of Strain Gauges

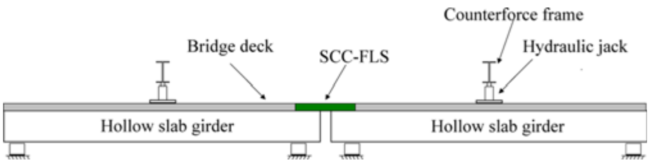


Fig. 21. Test Setup

Fig. 22. Test Loading Photo

points was shown in Figs. 19 and 20.

Two hydraulic jacks (Load stroke 50,000 kg) were applied at the midspan of the girder, which were used to simulate the lane load, the maximum loading was 144.9 kN, which was equivalent to lane load of highway I grade in Chinese code for design of highway reinforced concrete and prestressed concrete bridges and culverts. The schematic diagram and the photo of test loading device was shown in Figs. 21 and 22.

### 5.2 Test Results

The field test was loaded step by step (43 kN, 73 kN, 97 kN, 115 kN, 132.9 kN and 144.9 kN), and the strain of the measuring point and the deformation of the girder and link slab were measured during the loading process, Fig. 23 showed the stress curves of upper surface concrete.

From the figure, it can be seen that the stress of link slab concrete was compressive state of stress and increased with load, and the compressive stress under the maximum load was about -1.3 MPa. The test results showed that the link slab concrete was completely compressed under the mid span loads, which can

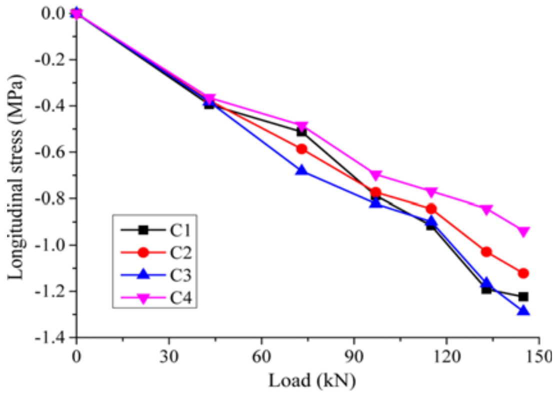


Fig. 23. Stress Curves of Upper Surface Concrete

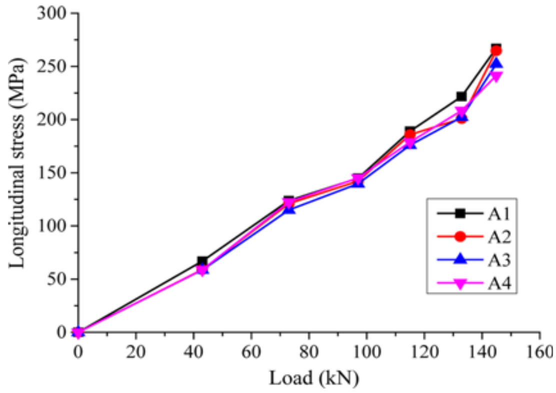


Fig. 24. Longitudinal Stress Curves of Welded Steel

prevent the concrete cracking of link slab.

According to the analysis, the stress mechanism of the SCC-FLS was as follows:

1. From the analysis above, the longitudinal tensile force on the link slab concrete was second failure factor of link slab destruction. Under the bridge load or temperature load, the horizontal tensile stress was passed directly to the link slab, the link slab concrete will not be able to withstand the stress and crack. Therefore, SCC-FLS changed the stress transmission path, so that the stress was transmitted through the welded rebar and steel concrete composite structure. Fig. 24 showed the stress curves of welded steel at the steel plate edge, the steel stress was up to 273.98 MPa, the stress was transferred to the SCC-FLS, because the steel concrete composite section stiffness was improved, so the strain was small, which did not exceed the ultimate tensile strength of concrete.
2. The welded rebars were arranged on the SCC-FLS below the section neutral axis, while sliding PTFE bearings were set, which produced positive bending moment and keep the link slab concrete in compression. Therefore, the SCC-FLS can prevent cracking of link slab concrete.

## 6. Conclusions

A new type of steel-concrete composite flat link slab was put forward with the followed verification by FEA and field test that it can avoid concrete cracking. Based on theoretical and quantitative analysis on traditional link slab structure, the following conclusions can be drawn that

1. The leading factor for link slab failure is the girder end upturning, followed by the longitudinally tension and the girder end rotation, respectively
2. The derived theoretical formulas can rather effectively analyze the stresses in link slab and rather accurately distinguish the effects of various destructive factors, which provides basis for the prevention and treatment of link slab cracking problem
3. The FEA and experimental results show that the proposed steel-concrete composite flat link slab can always keep the upper region of concrete of link slab in compression

## Acknowledgements

The authors appreciate the support from the fundamental research funds for the central universities (JUSRP11819), natural science foundation of Jiangsu Province (BK20180623), national natural science foundation of China (51378240, 51778147 and 51578161), 2018 science and technology department's social development project (BE2018625) and 2015 Jiangsu provincial building energy saving and construction industry science and technology project.

## References

Alampalli, S. and Yannotti, A. P. (1998). “In-service performance of integral bridges and jointless decks.” *Transportation Research Record*. No. 1624, pp. 1-7.

Attanayake, U. B., Ulku, A. E., and Aktan, H. M. (2008). “Structural system durability through jointless bridge decks.” *Proc. The 4th International IABMAS Conference*, Seoul, Korea, p. 239.

Au, A., Lam, C., Au, J., and Tharmabala, B. (2013). “Eliminating deck joints using debonded link slabs: Research and field tests in ontario.” *Journal of Bridge Engineering*, Vol. 18, No. 8, pp. 768-778, DOI: 10.1061/(ASCE)BE.1943-5592.0000417.

Badie, S. S., Tadros, M. K., and Pedersen, K. E. (2001). “Re-examination of I-girder/pier connection in jointless bridges.” *PCI Journal*, Vol. 46, No. 2, pp. 62-74, DOI: 10.15554/pcij.03012001.62.74.

El-Safty, A. (2008). “Extending the service life of bridges using CFRP laminates and continuous decks.” *PCI Journal*, Vol. 53, No. 6, DOI: 10.1061/41016(314)23.

Gastal, F. and Zia, P. (1989). *Analysis of bridge beams with jointless decks*, IABSE Report, Vol. 57/2, Iabse symposium, Lisbon, Portugal.

Ghatefar, A., El-Salakawy, E., and Bassuoni, M. T. (2015). “Early-age restrained shrinkage cracking of GFRP-RC bridge deck slabs: Effect of environmental conditions.” *Cement and Concrete Composites*, Vol. 64, pp. 62-73, DOI: 10.1016/j.cemconcomp.2015.07.010.

Hossain, K. M. A., Ghatrehsamani, S., and Anwar, M. S. (2015). “Flexural fatigue performance of ECC link slabs for bridge deck applications.” *Sustainable Bridge Structure*, NY, USA, p. 247.

Kendall, A., Keoleian, G. A., and Helfand, G. E. (2008). “Integrated life-cycle assessment and life-cycle cost analysis model for concrete bridge deck applications.” *Journal of Infrastructure Systems*, Vol. 14, No. 3, pp. 214-222, DOI: 10.1061/(ASCE)1076-0342(2008)14:3(214).

Lepech, M. D. and Li, V. C. (2009). “Application of ECC for bridge deck link slabs.” *Materials and Structures*, Vol. 42, No. 9, pp. 1185-1195, DOI: 10.1617/s11527-009-9544-5.

Li, F., Liu, X. Y., Wang, R. X., and Wang, X. W. (2012). “Mechanical analysis of link slab in continous paving layer of simple supported girder bridge.” *Applied Mechanics and Materials*, Vols. 178-181, pp. 2290-2293, DOI: 10.4028/www.scientific.net/AMM.178-181.2290.

Loveall, C. L. (1985). “Jointless bridge decks.” *Civil Engineering,* Vol. 55, No. 11, pp. 64-67.

Moradi, M., Valipour, H., and Foster, S. (2017). “Fatigue behaviour of transversely restrained precast steel fibre reinforced concrete slabs in a deconstructable composite deck.” *Construction and Building Materials*, Vol. 132, pp. 516-528, DOI: 10.1016/j.conbuildmat.2016.12.029.

Moradi, M., Valipour, H., Foster, S. J., and Bradford, M. A. (2016). “Deconstructable steel-fibre reinforced concrete deck slabs with a transverse confining system.” *Materials and Design*, Vol. 89, pp. 1007-1019, DOI: 10.1016/j.matdes.2015.10.059.

Natário, F., Fernández Ruiz, M., and Muttoni, A. (2015). “Experimental investigation on fatigue of concrete cantilever bridge deck slabs subjected to concentrated loads.” *Engineering Structures*, Vol. 89, pp. 191-203, DOI: 10.1016/j.engstruct.2015.02.010.

Oesterle, R. G., Mehrabi, A. B., Tabatabai, H., Scanlon, A., and Ligozio, C. A. (2004). “Continuity considerations in prestressed concrete jointless bridges.” *Proc. The 2004 Structures Congress*, Nashville, TN, USA, pp. 1-8.

Okeil, A. M. and Elsafty, A. (2005). “Partial continuity in bridge girders with jointless decks.” *Practice Periodical on Structural Design and Construction*, Vol. 10, No. 4, pp. 229-238, DOI: 10.1061/(ASCE)1084-0680(2005)10:4(229).

Pons, D., Espinos, A., Albero, V., and Romero, M. L. (2018). “Numerical study on axially loaded ultra-high strength concrete-filled dual steel columns.” *Steel and Composite Structures*, Vol. 26, No. 6, pp. 705-717, DOI: 10.12989/scs.2018.26.6.705.

Sevgili, G. and Caner, A. (2009). “Improved seismic response of multisimple-span skewed bridges retrofitted with link slabs”. *Journal of Bridge Engineering*, Vol. 14, No. 6, pp. 452-459, DOI: 10.1061/(ASCE)1084-0702(2009)14:6(452).

Strauss, A., Krawtschuk, A., Wendner, R., Frangopol, D. M., and Bergmeister, K. (2012). “Monitoring-based assessment of a jointless bridge.” *Conference of IABMAS 2012*, Stresa, Lake Maggiore, Italy.

Valipour, H., Rajabi, A., Foster, S. J., and Bradford, M. A. (2015). “Arching behaviour of precast concrete slabs in a deconstructable composite bridge deck.” *Construction and Building Materials*, Vol. 87, pp. 67-77, DOI: 10.1016/j.conbuildmat.2015.04.006.

Wang, H., Hu, C., and Wang, B. (2000). “Calculating analysis for the warpage and stress of deck pavement at tip position of assembly simple beam bridge.” *Journal of Xi'an Highway Transportation University*, Vol. 20, No. 4, pp. 1-3.

Wang, C., Shen, Y., Wang, G., and Xie, X. (2016). “Field tests on mechanical characteristic of link slab on hollow-cored slab beam bridge.” *Journal of Zhejiang University (Engineering Science)*, Vol. 50, No. 8, pp. 1438-1445, DOI: 10.3785/j.issn.1008-973X.2016.08.003.

Wang, C., Shen, Y., Wang, G., and Xie, X. (2016). “Field tests on mechanical characteristic of link slab on hollow-cored slab beam bridge.” *Journal of Zhejiang University (Engineering Science)*, Vol. 50, No. 8, pp. 1438-1445, DOI: 10.3785/j.issn.1008-973X.2016.08.003.

Wang, G., Xie, X., Wang, C., and Shen, Y. (2014). “Mechanical performance of arch-type continuous slab-deck on simply-supported girder bridge." *Journal of Zhejiang University (Engineering Science),* Vol. 48, No. 6, pp. 1049-1057, DOI: 10.3785/j.issn.1008-973X.2014.06.012.

Zhan, X. F., Shao, X. D., and Liu, G. L. (2013). "Thermal experiment of a reinforced approach pavement for semi-integral abutment jointless bridge." *Advanced Materials Research*, Vols. 639-640, pp. 183-190, DOI: 10.4028/www.scientific.net/AMR.639-640.183.

Zheng, Y., Zhang, L. F., and Xia, L. P. (2018). "Investigation of the behaviour of flexible and ductile ECC link slab reinforced with FRP." *Construction and Building Materials*, Vol. 166, pp. 694-711, DOI: 10.1016/j.conbuildmat.2018.01.188.